Experiments in Fluids (2022) 63: 151
https://doi.org/10.1007/s00348-022-03498-3

RESEARCH ARTICLE

Appraisal of cavity hot-wire probes for wall-shear-stress measurements

Adalberto Perez[1] · Ramis Örlü[1,2] · Alessandro Talamelli[2] · Philipp Schlatter[1,2]

Received: 11 March 2022 / Revised: 4 July 2022 / Accepted: 21 August 2022 / Published online: 15 September 2022

Abstract
Flush-mounted cavity hot-wire probes have emerged as an alternative to classical hot-wire probes mounted several diameters above the surface for wall-shear stress measurements. They aim at increasing the frequency response and accuracy by circumventing the well-known issue of heat transfer to the substrate that hot-wire and hot-film probes possess. Their use, however, depends on the assumption that the cavity does not influence the flow field. In this study, we show that this assumption does not hold, and that turbulence statistics are modified by the presence of the cavity with sizes that are practically in use. The mean velocity and fluctuations increase near the cavity while the shear stress decreases in its surroundings, all seemingly stemming from the fact that the no-slip condition is not present anymore and that flow reversal occurs. Overall, the energy spectra and the probability density function of the wall shear stress fluctuations indicate a change of nature of turbulence by the presence of the cavity.

1 Introduction

Hot-wire and hot-film anemometry have been extensively used to measure turbulence quantities since the end of the last century. While hot films can be directly mounted at the surface, hot-wire probes are typically positioned several wire diameters above the wall. Both techniques suffer from a well-known limitation of the sensitivity due to the heat transfer to the substrate, which reduces the accuracy for low wall-shear-stress scenarios. In order to reduce the heat transfer to the surroundings, flush-mounted (or cavity) probes, characterized by the presence of openings (or cavities) below the heated element (see Fig. 1), are often utilized (Örlü and Vinuesa 2020).

Different types of flush-mounted probes have been introduced over the years to measure important quantities in the near-wall region such as the mean wall-shear stress and its fluctuations. A cylindrical cavity with two parallel hot wires was used in Spazzini et al. (1999) to measure time-resolved wall shear stress and its direction for separated flows. In Sturzebecher et al. (2001), flush-mounted hot-wire probes were used in an array of rectangular cavities for the analysis of the development of Tollmien-Schlichting waves in transitional flows. More recently, Gubian et al. (2019) used a similar method to study the Reynolds-number dependency of the amplitude of the wall-shear-stress fluctuations. All of these methods are quite attractive since they involve the use of standard sensors and electronics. However, some assumptions must be introduced, namely that the shear stress over the cavity is equivalent to the wall shear stress one would have without the cavity (Spazzini et al. 1999). Even though these techniques have been, to some degree, validated, as stated in Spazzini et al. (1999), we believe that a detailed quantitative appraisal of the effect of introducing a cavity into the flow is of fundamental importance to ensure that errors introduced in the measurements, if any, can be properly estimated. To the best of the authors' knowledge, we have not come across a study that would remedy the statement by Spazzini et al. from two decades ago that "*there are no detailed studies in the literature dealing with the flow inside a cylindrical cavity in a flow regime similar to that of the present application*".

In this work we aim at evaluating the validity of the aforementioned assumptions introduced in Spazzini et al. (1999) and appraise the flow field that would be measured with a cavity hot-wire probe. In particular, in light of recent

✉ Adalberto Perez
adperez@kth.se

[1] SimEX/FLOW, Department of Engineering Mechanics, KTH Royal Institute of Technology, 100 44 Stockholm, Sweden

[2] Dipartimento di Ingegneria Industriale, Università di Bologna, 47 100 Forlì, Italy

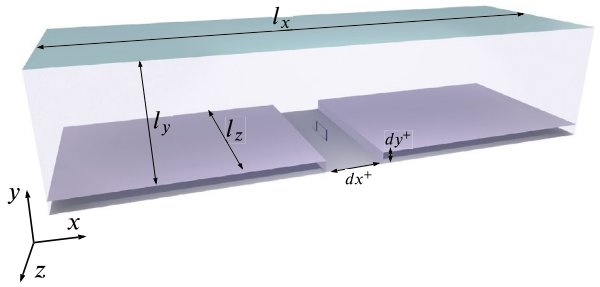

Fig. 1 Schematic of a cavity probe and simulation domain

studies in which this technique has been utilized to generate controversial results (Gubian et al. 2019; Örlü and Schlatter 2020), this has become a timely question. To accomplish this, Direct Numerical Simulations (DNS) of a channel flow with small cavities of sizes comparable to those used in experiments with cavity probes are performed by using techniques similar to previous works in which the performance of hot-wire probes was assessed through DNS, see e.g. Segalini et al. (2011) and Örlü et al. (2014). It should be noted that we are solely interested in the effect of the cavity on the flow field in order to test the assumptions that enable the use of cavity probes. Therefore, in the course of this study, thermal effects of a hot-wire probe will not be taken into consideration.

The paper is organized as follows. In Sect. 2, we present the simulation parameters and give details of the numerical method employed in the study. Section 3 follows with the results and discussion, while we present our conclusions in Sect. 4.

2 Simulation methodolody

2.1 Code description

Direct Numerical Simulations (DNS) were performed through the pseudo-spectral solver Simson (Chevalier et al. 2007), which time-integrates the Navier–Stokes equations in their velocity-vorticity formulation. With this implementation, no solution for the pressure term is needed, and relevant quantities can be collected directly.

The streamwise and spanwise directions are discretized using a Fourier transformation on a set of equally spaced grid points while the wall-normal direction, i.e. the non-periodic direction, is discretized employing a Chebyshev expansion. The temporal discretization uses a Crank–Nicholson method for the diffusion term and a Runge–Kutta method of third order for the convective one.

Spectral approximations have well-known limitations to model complex geometries and are often constrained to rectangular domains such as a channel. Due to this fact, the Immersed Boundary Method (IBM) described in Goldstein et al. (1993) was implemented to introduce the cavity into the simulations. In an equilibrium condition, fluids perceive the presence of a body through pressure and shear forces along its surface. IBM consists of introducing the appropriate body forces to model the no-slip and impermeability conditions on the boundaries of a given geometry by utilizing a control feedback loop as seen in Eq. (1).

$$F_i(x,y,z,t) = \alpha u_i(x,y,z,t) + \beta \int_0^t u_i(x,y,z,t)\mathrm{d}t. \tag{1}$$

In this case, α and β are calibration constants that need to be adjusted and serve as relaxation times of the method. They were selected by running trial cases and ensuring that correct statistics were obtained. More details on the implementation and validation are available in Alvisi and Perez (2020).

2.2 Simulation set-up

The simulation domain is the canonical channel flow with periodic boundary conditions on the streamwise and spanwise directions, and, as mentioned in Sect. 2.1, IBM was used to introduce the presence of the cavity. The exact manner in which this was achieved is seen in Fig. 1. Two immersed boundaries were introduced into the domain, such that the shape of a cavity would take form, having finite dimensions in the streamwise and wall-normal directions while being continuous across the spanwise one. The latter condition is a simplification of a real experimental set-up where a finite dimension in the spanwise direction would be used. This simplification is motivated by the fact that experimental cavities tend to be several times larger in the spanwise direction than they are in the streamwise and wall-normal one, therefore a 2D cavity approximates the behavior of such a case. The specific size of the domain and the tested cavity sizes can be seen in Table 1. The domain parameters have been provided as non-dimensional quantities, however, in order to give an easier assessment of the dimensions of the smallest cavity we study, the reader can consider the case where the channel half-height is $h = 30\,\mathrm{mm}$ and the center-line velocity is $U_{\mathrm{cl}} = 10\,\mathrm{m/s}$ of air. For such a case, $u_\tau = 0.43\,\mathrm{m/s}$ and the dimensions of the smallest cavity are $\mathrm{d}x = 2.5\,\mathrm{mm}$ and $\mathrm{d}y = 0.25\,\mathrm{mm}$. It should be noted, however, that the relevant expected dynamics are limited to the vicinity of the wall and characterized by inner units, which have been reported in Table 1.

At this stage, it is worth noting that the simulations in this study required much finer resolutions than a standard turbulent channel flow simulation. This is due to requirements introduced when using IBM. The particular settings

Table 1 Simulation domain and cavity sizes

Domain size				
l_x	$4\pi h$	l_x^+		2257
l_y	$2h$	l_y^+		359
l_z	$2\pi h$	l_z^+		1128
Cavity sizes				
Case	dx/h	dy/h	dx^+	dy^+
Ref.	0	0	0	0
1	0.0835	0.0084	15	1.5
2	0.1670	0.0084	30	1.5
3	0.1670	0.0167	30	3

The cavity sizes are given in (+), i.e. inner, units. Half-height of channel is h

are shown in Table 2. The appropriate number of grid points was selected based such that two conditions were fulfilled:

- **Condition A:** The statistical results are mesh independent.
- **Condition B:** The number of points are sufficient to generate the small cavities required with the IBM.

Several simulations were performed in Alvisi and Perez (2020) at a variety of resolutions to assess the impact of condition A. At this stage, it was found that the statistics and general flow behavior approached convergence with respect to mesh independence at a resolution of $n_x \times n_y \times n_z = 1024 \times 129 \times 160$. Having defined a baseline resolution, condition B takes relevance. The IBM consist of applying a forcing to the Navier–Stokes equations at each of the grid points, thus, to define a relatively small cavity, a large number of points must be present in the domain. The resolution presented in Table 2 is the result of analyzing the objective cavity size and selecting a resolution that would allow a proper representation of the geometry while ensuring an acceptable number of grid points are present in it.

The flow regime during the simulation is based on the friction Reynolds number $\mathrm{Re}_\tau = 180$ that, while being low, is sufficient for this study as the interest is small cavities with significant effects confined to regions close to the wall, i.e. the viscous sublayer, a region dominated by small scales, where the effect of large scales is not relevant, allowing the use of low Re simulations. A standard turbulent channel flow, i.e. without cavity, serves as the reference case to which the data from the channel with cavity will be compared against. In some cases, the data from the lower part of the channel, i.e. the side with the cavity, is compared to the upper smooth wall. For ease in the reading, we will henceforth refer to the upper wall as the reference wall.

2.3 Uncertainty quantification (UQ)

Numerical methods based on deterministic mathematical models are not exempt from uncertainty. Noting that uncertainty does not represent an error, but a lack of certainty in the value of a given quantity of interest, and can be caused by many sources such as the fidelity of the mathematical model, boundary conditions, sampling time, etc. (Oberkampf and Trucano 2002).

When collecting samples of a time series, a Sample Mean Estimator (SME) $\hat{\mu}$ can be used such that if enough data is collected, $\hat{\mu} \to \mu$, where μ is the true unobserved mean value of the quantity of interest. In general terms $\hat{\mu}$ will be normal distributed as $\hat{\mu} \approx \mathcal{N}(\mu, \sigma^2)$, where σ^2 is the variance and directly affects the uncertainty of the measurements. σ^2 is precisely the quantity to find when performing uncertainty analysis.

Table 2 Simulation set up

Grid points	
n_x	2048
n_y	201
n_z	160
Flow parameters	
Re_τ	179.6
u_τ/U_{cl}	0.0427

A particular challenge of finding mean values (SME) is the fact that for turbulent data the values are autocorrelated, thus the method must correctly deal with this characteristic. The uncertainty quantification in this study was implemented with resources from Rezaeiravesh et al. (2021). The used approach exploits an exact expression for σ^2 that depends on the autocorrelation of the SME. An additional challenge for UQ in the present study is that u_{rms} is not necessarily normal distributed and signals needed for its determination, e.g. u, u^2 are not independent.

3 Results and analysis

3.1 Flow field characterisation

The results presented will have an initial focus on case 3 of Table 1, for which most data was collected to elaborate a deeper analysis. For an initial assessment, the analysis was performed at two particular locations in the channel, i.e. at the streamwise location that corresponds to the center of the cavity (where the hot-wire would be placed in an experimental realization of a cavity probe), and far downstream from it. The main focus of this assessment is to determine if there is any direct effect of the cavity on the mean flow.

The aim of analyzing the two locations was to evaluate the physical effect of the cavity while investigating the impact of the computational method that generates it. On a section of the channel flow where the cavity does not have any effect, it is expected that the IBM would produce results identical to those of a reference case with no immersed surface, while any direct effect of the cavity should be seen at the appropriate location. This is what appears in Fig. 2, where we show the reference case, the profile of the upper half of the channel (channel section without cavity and immersed boundary, also denoted as the reference wall) and the wall generated by the IMB. While the turbulence statistics far from the cavity are indistinguishable between the cavity and reference case, the profile at the center of the cavity shows a clear deviation, underlining the effect of the cavity. The increase in U^+ and u^+_{rms} can be attributed to the lack of the no-slip condition at the location where the wall would be in absence of the cavity.

Figure 3 shows the confidence intervals for the turbulence statistics (multiplied by 5 for clarity) in the near-wall region for case 3 and compares them to the values of the reference case. It is apparent that the differences close to the wall are clearly not a product of uncertainties but undoubtedly stem from the presence of the cavity.

The seen differences can be further explained by understanding of the flow pattern inside the cavity, which can be achieved by employing a visualization of a streamwise 2D plane of the mean velocity, as shown in Fig. 4. In the figure,

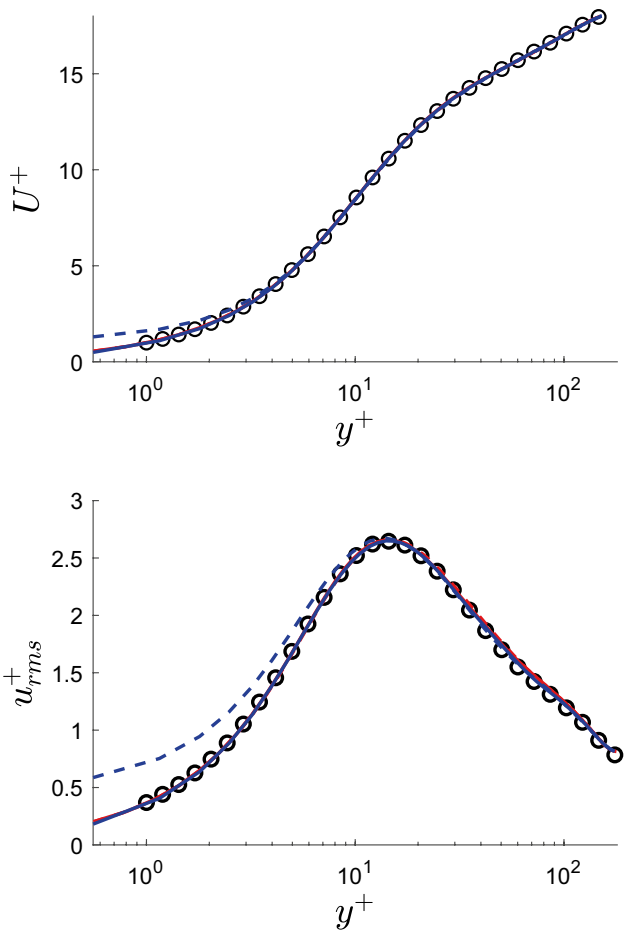

Fig. 2 Mean and rms profiles of the streamwise velocity component for the reference case (o), case 3 at cavity center (– –) and downstream from it (– –). The half channel for the reference wall is indicated with solid lines

we can observe how the streamlines are deflected towards the cavity and how a recirculation zone, a feature typical in cavities of larger scales, is formed for this case with a relatively small cavity size.

The behaviour of the rms values is very similar to the one observed for the mean, and can be more completely analyzed when considering the turbulence intensity ($T_u = u_{\mathrm{rms}}/U$) at the center of the cavity, shown in Fig. 5. It is clear from the figure that the fluctuations acquire higher dominance in the flow close to the cavity, and that the behaviour is dependent on the (inner-scaled) cavity size. Our observations indicate that the flow tends to separate at the start of the cavity and potentially reattaches inside (see Fig. 4), depending on the geometry. This explains the increased fluctuation levels in the shear layers, as this is a known characteristic of separated flows as seen by, among others, Simpson (1989) and Skote and Henningson (2002). Evidence indicates that due to the low momentum close to the wall, the flow would "feel" the presence of the cavity, as one might initially assume. This

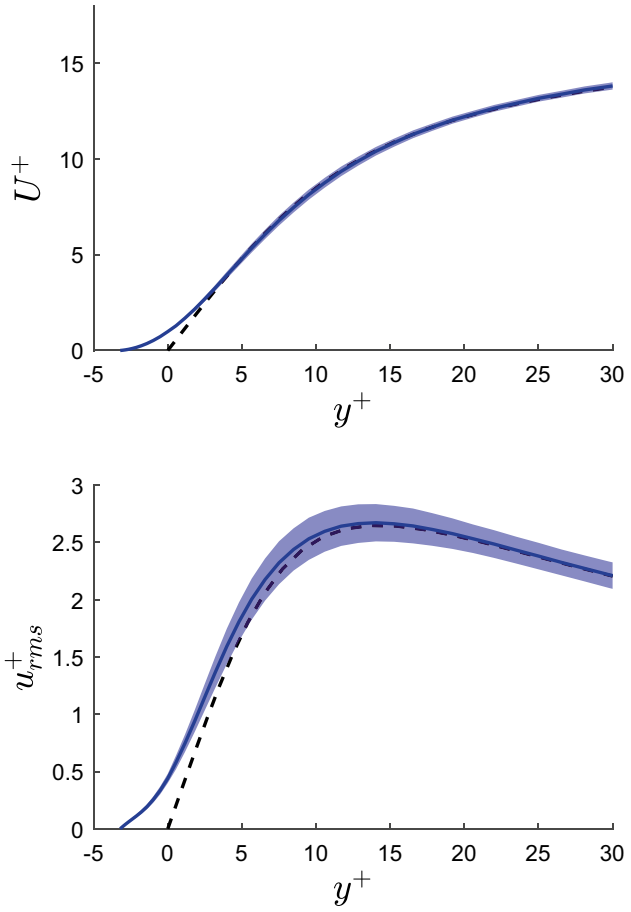

Fig. 3 Mean profiles and fluctuations of the streamwise velocity component for case 3. The shaded area represents the uncertainty computed with 95% confidence (multiplied by 5). Reference wall (- -)

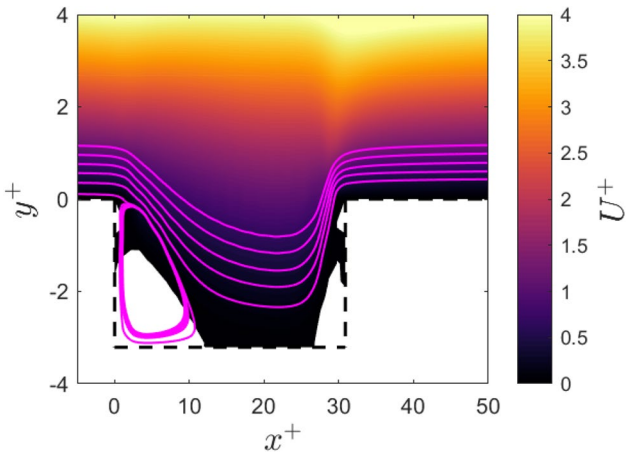

Fig. 4 Effect of the cavity in the mean velocity field and streamlines computed for case 3

behaviour appears to be dependent on the aspect ratio of the cavity where, depending on the length, the re-circulation

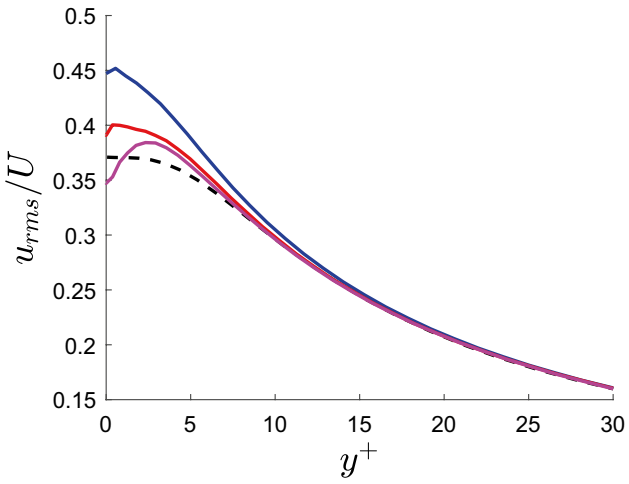

Fig. 5 Turbulence intensity for all studied cases. Case 1 (—), case 2 (—), case 3 (—) and reference case (- -)

zone seen in Fig. 4 might instead be present over the cavity. The effect of this culminates in an increase in the fluctuation level close to the cavity (see Fig. 7).

The sudden reduction in turbulence intensity for case 1 seen in Fig. 5 can be explained by further analyzing the flow patterns inside the cavity. For each case, a similar behavior was found, consisting of zones of high turbulence intensity close to the cavity walls and low-intensity just before the cavity's end, produced by the flow accelerating to exit the cavity. For case 1, the low intensity region at the exit happens to be very close to the location where the probe is located, as seen in Fig. 6. Independent of the numerical result, there is no doubt that the field is affected.

In the analysis that we have carried out, we have mentioned the dependence of the cavity effect to the geometry, and we have shown measures of this relation in Fig. 5, however, this knowledge can be extended by analysing the turbulence intensity at the cavity center for multiple cavity sizes. Figure 7, shows the variation of turbulence intensity with respect to the aspect ratio of the cavity (length/depth), which was chosen to be an appropriate measure of the cavity geometry. It is possible to observe from the figure how for constant aspect ratio, the deeper cavity would have a higher effect in the flow and that, in general, larger cavities would have increased effects as would be expected given the information of Fig. 4. Additionally, we found that for low aspect ratios the re-circulation zone tends to take over the cavity, while for longer cavities, the shear layers are able to reattach inside and the turbulence intensity level start to decrease.

3.2 Spectral analysis

A deeper understanding of the effect on the turbulence statistics and velocity fluctuations can be achieved by analyzing

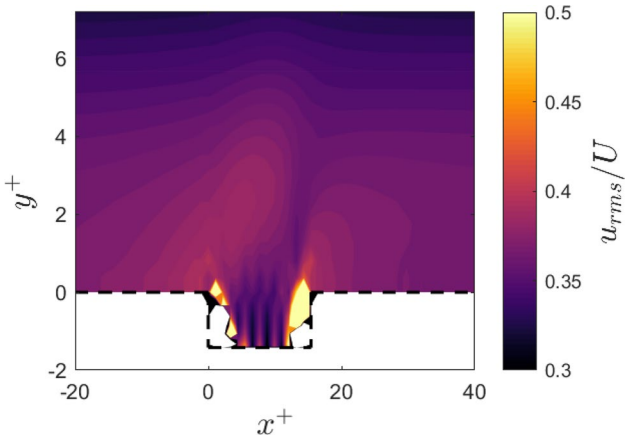

Fig. 6 Effect of the cavity on the streamwise turbulence intensity for case 1

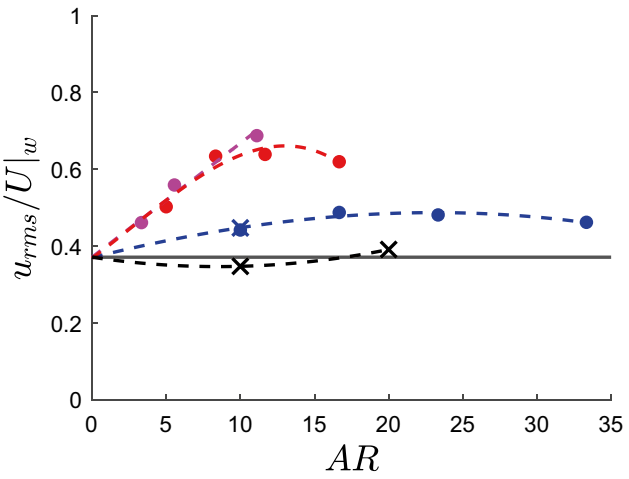

Fig. 7 Variation or the streamwise turbulence intensity for different aspect ratio of the cavity. (colored dots) simulation by Alvisi and Perez (2020) for different cavity depths: (•) $dy^+ = 3$, (•) $dy^+ = 6$, (•) $dy^+ = 9$, (—) reference case. Current simulations presented as crosses, (×) $dy^+ = 1.5$, (×) $dy^+ = 3$

the turbulence energy in the flow. For this purpose, we calculated the premultiplied power-spectral density (PSD) at a zy-plane at the streamwise location of the cavity center, seen in Fig. 8 for time and space. The data obtained matches qualitatively very well with the information presented in Eitel-Amor et al. (2014), and it is possible to observe that a maximum in spectral energy can be seen at a wall distance $y^+ \approx 12$ for a wavelength $\lambda_z^+ \approx 120$, which corresponds to the characteristic streak spacing in wall-bounded flows. For our case, given the low Reynolds number, we do not observe the typical second peak appearing a higher wave-lengths.

These findings indicate that the general nature of turbulence, i.e energy content of the scales away from the wall, is not severely affected by the presence of the cavity. When comparing the PSD of the top and bottom wall, clear differences are appreciated at lower wall-normal distances, where the side with a cavity possesses more energy which is an expected result, since the no-slip condition is not in place at the lower wall, allowing for the rise in the values of U^+ and u^+_{rms}. The power spectral density in space also allows to increase the validity of the low Reynolds number simulations, since it is apparent that the higher energy seems concentrated at smaller scales, while the energy contents for higher wave-lengths is not significantly affected, i.e. the effect is localized to small eddies, as initially expected.

As mentioned in Sect. 2.2, an experimental set-up of a cavity probe would posses a finite width in the spanwise direction. Given that with the current conditions of the simulations there are no relevant differences in the energy content in the spectrum, we do not expect to see any changes in an experimental realization of the study.

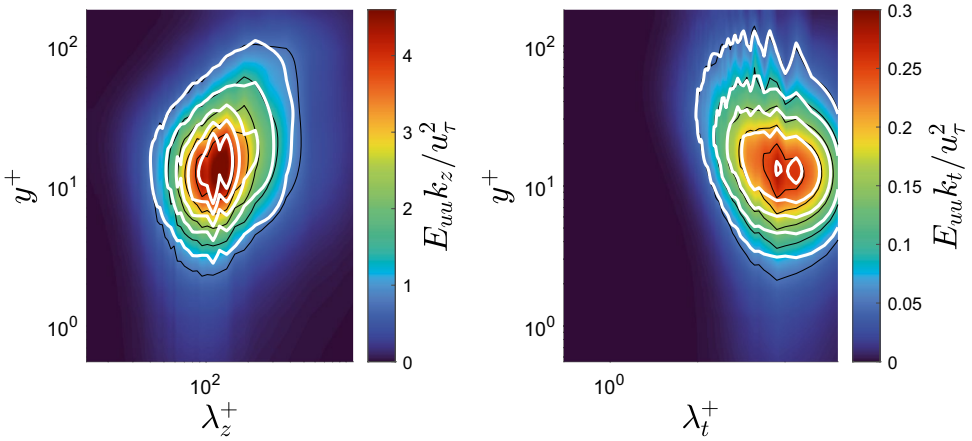

Fig. 8 Pre-Multiplied Power Spectral Density in space (left) and time (right). White lines correspond to contours of the PSD on the half channel of the reference wall

3.3 Wall shear-stress statistics

The obvious and foremost use of cavity probes is to measure in the immediate vicinity of the wall. For this reason, we evaluate the effect of the cavity not only on the mean and fluctuation velocity but also in terms of the fluctuating wall shear stress. From a computational field it is possible to calculate the stress directly from the derivatives of the velocity as follows:

$$\tau^+ = \frac{\partial U^+}{\partial y^+} = \frac{\nu}{u_\tau^2}\frac{\partial U}{\partial y} = \frac{\tau}{\tau_w}, \tag{2}$$

$$\tau^+_{\mathrm{rms}} = \sqrt{\left\langle \left(\frac{\partial u'^+}{\partial y^+}\right)^2 \right\rangle} = \frac{\nu}{u_\tau^2}\sqrt{\left\langle \left(\frac{\partial u'}{\partial y}\right)^2 \right\rangle} = \frac{\tau_{\mathrm{rms}}}{\tau_w}. \tag{3}$$

Note that the scaling factor τ_w comes from the definition of u_τ. While the mean wall-shear stress τ_w is a time and space averaged quantity in a periodic channel flow, this is not the case if a cavity is included, as it is also affected by its presence, as apparent from Fig. 9. The shear stress is reduced at the center of the cavity, which is due to the absence of the no-slip condition at the height where the wall would have been. It is noted, that the values of the normalized shear stress presented in Fig. 9 have been scaled by the same τ_w in all cases, in order to provide meaningful comparisons.

Without cavity, the normalized wall shear stress fluctuations can be indirectly measured, as stated in Alfredsson et al. (1988), employing a near-wall Taylor expansion of the velocity fluctuations,

$$u'^+ = u'^+|_w + \left.\frac{\partial u'^+}{\partial y^+}\right|_w y^+. \tag{4}$$

This is a linear function, where the slope corresponds to the normalized wall shear stress fluctuations as seen in Eq. (3). Since it is known that in the near-wall region $y^+ = U^+$, and for a case with the no-slip condition, from Eq. (4) follows

$$\tau^+_{w,\mathrm{rms}} = \lim_{y\to 0}\frac{u^+_{\mathrm{rms}}(y^+)}{U^+(y^+)}. \tag{5}$$

In Örlü and Schlatter (2011) and Alfredsson et al. (2011) and references therein $\tau^+_{w,\mathrm{rms}}$ is around 0.4 as shown in agreement with Alfredsson et al. (1988), but exhibits a clear Reynolds-number dependence. This Re-trend extends from the wall further outwards encompassing the near-wall peak in the streamwise variance profile (Smits et al. 2021). Equation (5) is the most convenient way to experimentally deduce the wall shear stress fluctuations since all the information can be retrieved from the signal captured by the probe. The turbulence intensity has been show in Fig. 5 for all the cases

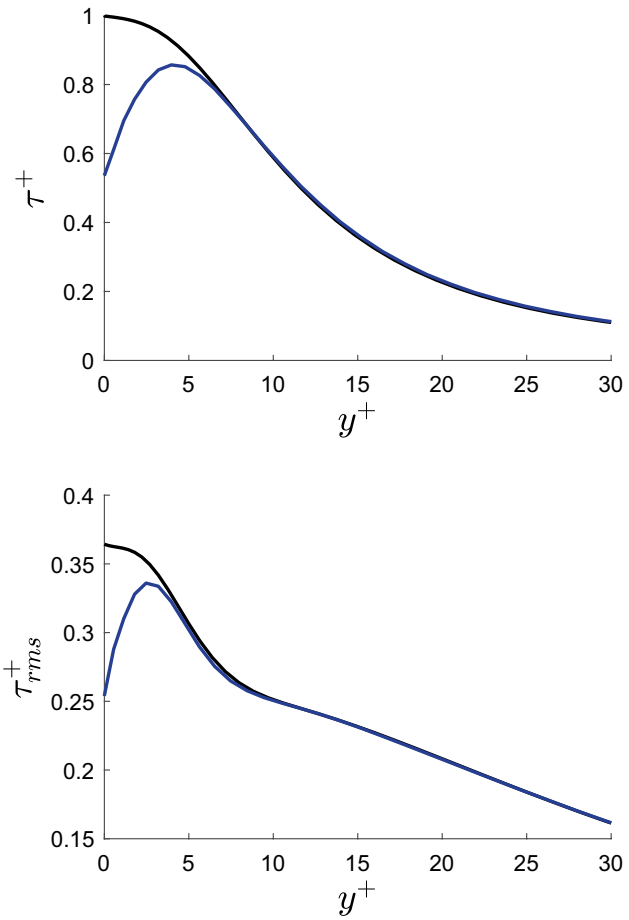

Fig. 9 Mean and rms distribution of the shear stress fluctuations in the channel for case 3. (—) reference wall, (—) cavity center

in Table 2. It is clear that at the center of the cavity, relation 5 would overpredict the normalized wall shear stress fluctuations seen in Fig. 9 for the cavity side. In this case, the clear explanation of the invalidity of (5) at the cavity center is that, as mentioned in previous sections, the no-slip condition is not valid over the cavity, and $U^+ \neq y^+$ close to $y^+ = 0$ (see Figs. 2 and 3).

If desired, indirect measurements can still be performed by lifting the restrictions placed to Eq. (5), extending it as

$$\tau^+_{w,\mathrm{rms}} = \lim_{y^+\to 0}\frac{u^+_{\mathrm{rms}}(y^+) - u^+_{w,\mathrm{rms}}}{y^+}. \tag{6}$$

Results using Eq. (6) are shown in Fig. 10. However the usability of the method is questionable since the real wall shear stress is reduced by the cavity. Ideally, some form of correction factor could be created in order to account for the presence of the cavity, however, it should be noted that this is highly dependent on the practical implementation of the cavity.

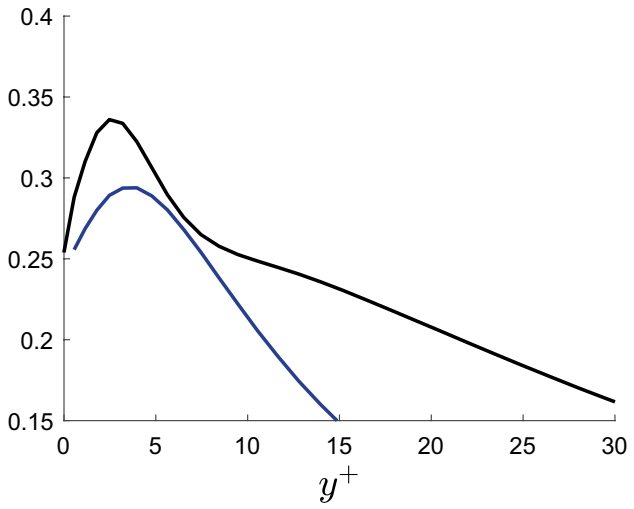

Fig. 10 Comparison of original data and experimental approximation. (—) Distribution of shear stress in case 3, (—) function obtained from (6)

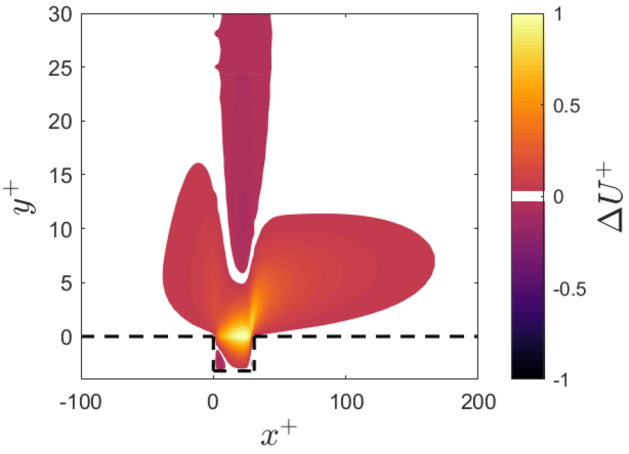

Fig. 11 Difference between the computed mean velocity and the velocity profile at the inlet of the channel

3.4 Effects of the cavity in its surroundings

From the information in Figs. 2 and 5, it is possible to observe that the influence of the cavity is not confined to measurements at the immediate vicinity of the cavity, but affects wall-normal distances far beyond the viscous sublayer. The effect is, however, more prominent in the velocity fluctuations than in the mean, as evidenced in the increase of the turbulence intensity.

The effects are not necessarily confined to the wall normal direction. For this reason, it is also interesting to determine how the cavity effects extend in the streamwise direction. This is relevant because, at high Reynolds numbers, even small irregularities on wind tunnel surfaces would achieve sizes comparable to the ones explored in this study. To assess the region of influence of the cavity, the following quantity has been calculated:

$$\Delta U^+ = U^+(x^+, y^+) - U^+(y^+)|_{inlet} \tag{7}$$

In this case, ΔU^+ represents the absolute difference between the mean velocity of the field and the velocity profile at the inlet of the channel. In the canonical channel flow, the difference must be equal to zero in the homogeneous direction, however, to measure the effect of the cavity, in Fig. 11 we show ΔU^+ for every point where the difference is larger than the average uncertainty while calculating the mean, thus, it allows to visualize where the main differences are concentrated.

From the figure, it is apparent that there are clear and large differences at the cavity location, however, is it also evident that the presence of the cavity modifies the flow field considerably in the streamwise direction. It is interesting to see that the influence can be felt up to one and 5 cavity length upstream and downstream, respectively. It should be noted that the results here can not be transferred one-to-one to a spanwise limited cavity. Nonetheless, it is found that the effect of the cavity replicates experimental observations.

3.5 Spatial resolution effects

The effect of cavities on the velocity field and shear stress have been shown, however, when performing experiments using this method other short comings of using hot-wire probes might as well come into play. For this purpose we investigate how the combined effect of measurement errors would propagate. We choose to evaluate the effects of insufficient spatial resolution when paired with cavity probes.

Hutchins et al. (2009) demonstrated how the small scale contribution to the velocity profile is mostly felt at low y^+ values, i.e. close to walls, where the smallest scales and turbulence are produced. If the probe size is not small enough to resolve these scales, an attenuation in the velocity fluctuations will be obtained in the measurements. This kind of limitation is known as l^+ effects, and it is an artifact produced by inadequate sensor length for a given flow condition, which has been studied extensively in the last decade (Örlü and Alfredsson 2010; Segalini et al. 2011; Chin et al. 2009; Miller et al. 2014; Gatti et al. 2022), cf. review in Örlü and Vinuesa (2017).

Since the nature of the effect is the averaging over the smaller scales, it is possible to reproduce its effect through the numerical data set if a top-hat filter is applied. This results in the values of the fields to be averaged over a given span l^+. The outcomes of applying this procedure to the data set for study case 3 are shown in Figs. 12 and 13. We now clarify that we have deemed $\tau^+_{w,\mathrm{rms}} = \tau_{w,\mathrm{rms}}/\tau_{w,\mathrm{ref}}$, where we

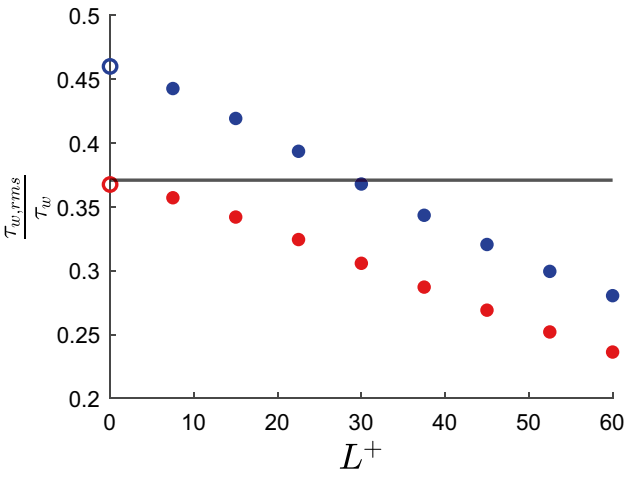

Fig. 12 Variation of the ratio of the mean and rms wall shear stress for different averaging. (•) cavity center, (•) reference wall, (—) expected value from unfiltered data

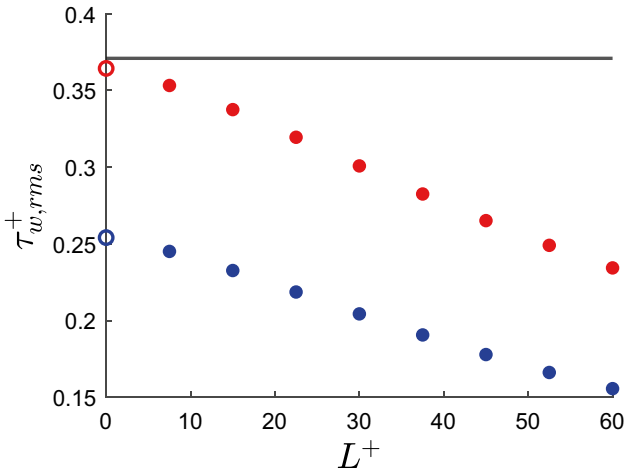

Fig. 13 Variation of the normalized wall shear stress fluctuations for different averaging. (•) cavity center, (•) reference wall, (—) expected value from unfiltered data

scale the rms values on the cavity and reference walls by the same value of the mean. In Fig. 12, we show the scaling of the rms values with the local means of the wall shear stress (which, as shown in Fig. 9 are different, between the cavity and reference wall).

From Fig. 12 it can be seen that the measured $\tau_{w,\mathrm{rms}}/\tau_w$ is higher on the cavity side than the reference case when unfiltered since fluctuation levels are higher at the cavity center. The value then progressively decreases as the spatial effect worsens. At $l^+ \approx 30$ the overestimated $\tau_{w,\mathrm{rms}}/\tau_w$ at the cavity center would reduce to the reference value thereby exhibiting a cancellation of two measurement inefficiencies/errors. Such a "cancellation of effects", can—depending on flow conditions—reverse trends or even mask errors. From Fig. 13 an interesting fact appears, which is that the wall shear stress fluctuations, directly calculated from the gradients of the flow field (no experimental relation used), are also attenuated by spatial averaging. This is expected from a mathematical standpoint, as attenuating the values would undoubtedly produce smaller gradients in the field. In general, any quantity that directly or indirectly depends on the velocity would suffer from the same phenomenon.

3.6 Experimental implications

Cavity probes as well as wall-mounted hot-wires and hot-films can be calibrated either *ex situ* or *in situ*. While *ex situ* calibrations are often performed in a well-defined laminar flow field, *in situ* calibration are often preferred when unknown mean flow features should be accounted for by means of the calibration. The established recirculation zone set up in non-negligible cavity sizes as shown in Fig. 4 highlights the importance of *in situ* calibrations, which would account for the biased mean wall-shear stress. Higher-order moments, as demonstrated on $\tau^+_{w,\mathrm{rms}}$ in Fig. 7 for realistic cavity sizes, can, however, not be accounted for due to the non-linearity of the flow.

Assuming now that either the cavity probe has been calibrated *in situ* or by neglecting the absolute value of the wall-shear stress, we can consider the normalized probability density function (PDF) of the wall-shear-stress fluctuations. This can e.g. been witnessed when considering the PDF from a cavity probe measured in Gubian et al. (2019) and reprinted here (Fig. 14). The used scaling by the rms value, which in itself can be biased, indicates that errors would to a large extent be cancelled out. The overlaid results from our cavity simulations agree very well with the data by Gubian et al. (2019), both for the reference, i.e. smooth channel, at their lowest Re data as well as for our case 3 (center of the cavity) with all of their other Re cases. Hence, regardless of whether the mean wall-shear stress is measured correctly or not, the measured PDF is not representative of that of a flow without a cavity. This can furthermore be underlined by considering the skewness and flatness factors of the wall-shear stress fluctuations.

As apparent from Table 3, literature values for the rms, skewness factor and flatness factor of the fluctuating wall-shear stress of a smooth channel flow agree well with those from the upper wall of the present simulation, here denoted as reference case. Conversely, the statistics collected from the center of the cavity, as was also the case for the PDF, agree reasonable well with the measurements of Gubian et al. (2019), which provide unique measurements with a cavity probe. It should be noted, however, that the lowest Reynolds number case of Gubian et al. (2019) is closer to that of a smooth wall, since the cavity has a depth of less

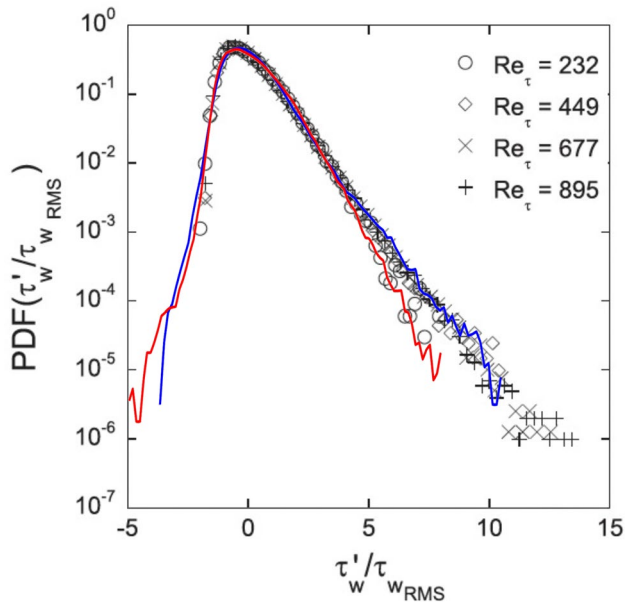

Fig. 14 Normalized probability density functions (PDFs) of the wall-shear stress fluctuations measured by a cavity probe (Gubian et al. 2019). Reprinted with permission from the American Physical Society. Overlaid on the original figure from Gubian et al. (2019) are the PDFs for the present simulation of case 3 for both the reference wall (—) and the cavity center (—)

Table 3 Comparison of statistics of the fluctuating wall-shear-stress for turbulent channel flows

Reference	Re_τ	$\tau^+_{w,\mathrm{rms}}$	$S(\tau_w)$	$F(\tau_w)$
Smooth channel simulations				
Lenaers et al. (2012)	180	0.37	0.93	4.22
Lenaers et al. (2012)	590	0.40	1.01	4.80
Lenaers et al. (2012)	1000	0.42	1.06	5.10
Present channel simulation				
Case Ref. (upper wall)	180	0.36	0.98	4.43
Case 3 (cavity side)	180	**0.45**	**1.30**	**6.71**
Cavity probe experiments in a channel				
Gubian et al. (2019)	232	**0.28**	**1.13**	**4.93**
Gubian et al. (2019)	564	**0.44**	**1.41**	**6.60**
Gubian et al. (2019)	954	**0.44**	**1.40**	**6.38**

Values in bold refer to results from the cavity center

than one viscous unit, which in agreement with Fig. 7, has a negligible error on the statistics.

We also note that even while neglecting any 3D effect of the cavity, we are able to correctly characterize the PDF of an experimental signal, which allows us to conclude that our simulation is representing correctly the local flow in the cavity despite the initial assumption of considering a spanwise continuous cavity.

4 Conclusions and future work

In this study, DNS of a periodic turbulent channel flow at $Re_\tau \approx 180$ with different cavity sizes, replicating the cavities used for cavity hot-wire probes, were performed. It was found that besides changes in the mean flow also the fluctuation levels increase inside and around the cavity. With this information, the assumptions that motivated the use of flush-mounted cavity probes are shown to not hold for the cavity sizes studied in this study. It was shown that seemingly correct values might be obtained through the combination of insufficient spatial resolution effects. Overall the flow is changed in the cavity vicinity and several cavity lengths downstream. Hence, any study performed with the use of this method must consider all these limitations and the results must be regarded with care depending on the application, in particular, if higher moments of the fluctuating wall-shear stress and high accuracy of its mean is required. Cavity probes should therefore be used with caution, in particular when utilizing them to study Reynolds-number effects since the cavity size and hot-wire length would change in viscous units as function of Reynolds number. This makes cavity probes—despite their comparably high frequency response compared to standard wall-mounted thermal anemometry probes—impractical for both quantitative and qualitative measurements without any proper error appraisal as initiated herein. Comparisons with existing experimental data from a cavity probe for the rms, skewness and flatness factors and hence PDF of the wall-shear-stress fluctuations, show that these results agree better with our cavity simulation than with those from a smooth channel flow.

Future work would be related to performing cavity simulations for higher Reynolds numbers, with the aim of characterizing an appropriate correction scheme to account for the errors sources described here. This is in particular of interest, since cavity probes are still of interest due to their high temporal resolution.

Acknowledgements This research was conducted using the resources of High Performance Computing Center North (HPC2N). The computations were enabled by resources provided by the Swedish National Infrastructure for Computing (SNIC), partially funded by the Swedish Research Council through grant agreement no. 2018-05973. Financial support by the Knut and Alice Wallenberg Foundation is gratefully acknowledged. Dr. Saleh Rezaeiravesh is acknowledged for fruitful discussions regarding UQ.

Funding Open access funding provided by Royal Institute of Technology.

Declarations

Competing interests The authors have no conflicts of interest to declare that are relevant to the content of this article.

References

Alfredsson PH, Johansson AV, Haritonidis JH, Eckelmann H (1988) The fluctuating wall-shear stress and the velocity field in the viscous sublayer. Phys Fluids 31:1026–1033

Alfredsson PH, Örlü R, Schlatter P (2011) The viscous sublayer revisited-exploiting self-similarity to determine the wall position and friction velocity. Exp Fuids 51:271–280

Alvisi A, Perez A (2020) Analysis of wall-mounted hot-wire probes. Master's thesis, KTH, Fluid Mechanics and Engineering Acoustics

Chevalier M, Schlatter P, Lundbladh A, Henningson DS (2007) SIMSON: A pseudo-spectral solver for incompressible boundary layer flows. Technical Report 2007:07, KTH, Mechanics

Chin C, Hutchins N, Ooi A, Marusic I (2009) Use of direct numerical simulation (DNS) data to investigate spatial resolution issues in measurements of wall-bounded turbulence. Meas Sci Technol 20(11):115401

Eitel-Amor G, Örlü R, Schlatter P (2014) Simulation and validation of a spatially evolving turbulent boundary layer up to $Re_\theta = 8300$. Int J Heat Fluid Flow 47:57–69

Gatti D, Stroh A, Frohnapfel B, Örlü R (2022) Spatial resolution issues in rough wall turbulence. Exp Fluids 63:63

Goldstein D, Handler R, Sirovich L (1993) Modeling a no-slip flow boundary with an external force field. J Comp Phys 105:354–366

Gubian PA, Stoker J, Medvescek J, Mydlarski L, Baliga BR (2019) Evolution of wall shear stress with Reynolds number in fully developed turbulent channel flow experiments. Phys Rev Fluids 4:074606

Hutchins N, Nickels TB, Marusic I, Chong MS (2009) Hot-wire spatial resolution issues in wall-bounded turbulence. J Fluid Mech 635:103–136

Lenaers P, Li Q, Brethouwer G, Schlatter P, Örlü R (2012) Rare backflow and extreme wall-normal velocity fluctuations in near-wall turbulence. Phys Fluids 24(3):035110

Miller M, Estejab B, Bailey S (2014) Evaluation of hot-wire spatial filtering corrections for wall turbulence and correction for end-conduction effects. Exp Fluids 55(5):1735

Oberkampf WL, Trucano TG (2002) Verification and validation in computational fluid dynamics. Prog Aerosp Sci 38:209–272

Örlü R, Alfredsson PH (2010) On spatial resolution issues related to time-averaged quantities using hot-wire anemometry. Exp Fuids 49:101–110

Örlü R, Schlatter P (2011) On the fluctuating wall-shear stress in zero pressure-gradient turbulent boundary layer flows. Phys Fluids 23:021704

Örlü R, Schlatter P (2020) Comment on "Evolution of wall shear stress with Reynolds number in fully developed turbulent channel flow experiments". Phys Rev Fluids 5:127601

Örlü R, Vinuesa R (2017) Thermal anemometry. In: Discetti S, Ianiro A (eds) Experimental aerodynamics. CRC Press Taylor & Francis Group, Boca Raton

Örlü R, Vinuesa R (2020) Instantaneous wall-shear-stress measurements: advances and application to near-wall extreme events. Meas Sci Technol 31:112001

Örlü R, Malizia F, Cimarelli A, Schlatter P, Talamelli A (2014) The influence of temperature fluctuations on hot-wire measurements in wall-bounded turbulence. Exp Fluids 55:1781

Rezaeiravesh S, Vinuesa R, Schlatter P (2021) Uqit: a python package for uncertainty quantification (UQ) in computational fluid dynamics (CFD). J Open Sour Softw 6(60):2871

Segalini A, Örlü R, Schlatter P, Alfredsson PH, Rüedi JD, Talamelli A (2011) A method to estimate turbulence intensity and transverse Taylor microscale in turbulent flows from spatially averaged hot-wire data. Exp Fluids 51:693–700

Simpson RL (1989) Turbulent boundary-layer separation. Annu Rev Fluid Mech 21:205–232

Skote M, Henningson DS (2002) Direct numerical simulation of a separated turbulent boundary layer. J Fluid Mech 471:107–136

Smits AJ, Hultmark M, Lee M, Pirozzoli S, Wu X (2021) Reynolds stress scaling in the near-wall region of wall-bounded flows. J Fluid Mech 926:A31

Spazzini PG, Iuso G, Onorato M, Zurlo N (1999) Design, test and validation of a probe for time-resolved measurement of skin friction. Meas Sci Technol 10(7):631

Sturzebecher D, Anders S, Nitsche W (2001) The surface hot wire as a means of measuring mean and fluctuating wall shear stress. Exp Fluids 31:294–301